C-band Microwave Backscatter of Sea Ice in the Weddell Sea during the Winter of 1992

Mark R. Drinkwater — Jet Propulsion Laboratory, California Institute of Technology, 4800 Oak Grove Drive, PasadcnuCA91109

Reza Hosseinmostafa — Remote *Sensing* Laboratory, University of Kansas, 2291 Irving Hill Road, Lawrence, Kansas 66045-2969

and Wolfgang Dierking — Alfred Wegener Institut für Polar und Meersforschung, Am Handelshaven 12, Bremerhaven, Germany

Abstract - A C-band radar was used to record the backscatter of Antarctic Weddell Sea ice in the w-inter of 1992. These shipbomc microwave signatures arc the first of their kind. Calibratedhh and vv-pol signatures were recorded for several ice types as the icebreaker crossed the Weddell Sea, At each site, measurements were made of snow and sea ice characteristics, Meteorological information, radiation budget and oceanographic data were also recorded. A fret-year icc result is presented with relation to the sea ice physical properties. In-situ data arc used in predictions from a theoretical model and the results compared with σ^o values. The primary scattering contributions under cold winter conditions come from the air/snow and snow/ice interfaces. Tlmc-series data indicate C-band is sensitive to snow and icc physical changes as a result of climatic and oceanographic forcing.

1. INTRODUCTION

Spaceborne microwave remote sensing is required to monitor the extent and characteristics of winter Antarctic sea ice, In this paper we begin to develop techniques to usc microwave radar signature data, During a 1992 austral winter experiment, sea ice scatterometer measurements were made together with surface measurements such that direct links between physical, chemical and dielectric properties of the sea ice and the surface flux *regime* could be determined. As a part of the Winter Weddell Gyrc Study (WWGS'92), a C-band scatterometer was operated from the port rail of the German research vessel F/S *Polarstern* to obtain the first shipborne scans of the microwave backscatter properties of Antarctic sca ice, The dual-polarization radar collected like- (w) and cross-polarized (hv) data at incidcncc angles from 15-65°. When stationary in pack ice, the radar was scanned to obtain independent samples of sea-ice backscatter (σ^o) as a function of incidence angle (6) and polarization. Field sampling provided validation data for simultaneous satellite ERS- 1 C-band SAR observations (at θ=23°) and enabled collection of a catalogue of 'snap-shot' microwave signatures. *In* support, detailed surface measurements were made within the radar footprint each time a radar scan was completed.

Short 3-4 hour ice stations shown in Fig. 1 enabled radar and snow and ice measurements of a number of icc types characteristic of the winter Weddell Sca ice cover [1]. A 3-day long ice station from 21-24 July, 1992 also enabled time-scncs σ^o measurements. In addition to periodic scans of data over the complete range of incidcncc angles, the radar was operated at frequent intervals (- 4 hourly) at θ=45°. At this angle σ^o is sensitive to rhc surface reflectivity and roughness, and also to volume scattering within rhc snow and ice surface. These data provide a chance to quantify changes in o" as the heat flux and vapour flux regime varied over the period, and as the physical properties of the snow and ice changed.

2. SENSOR DESCRIPTION

The field sensor was a frequency-modulated, continuous-wave (FM-CW) radar, modified from a King airborne radar altimeter. (see Table 1). The antenna cluster consisted of parabola for transmitting; a horn antenna for receiving linear like-polarized signals; and an alternate receiving antenna for cross-polarized signals. A steerable mount was secured to the port rail of the upper deck, orthogonal to rhc ship's centerline. It was fixed m azimuth but hinged m the elevation plane arrd driven using an actuator. A electronic pendulum gave a simple digital readout from which θ

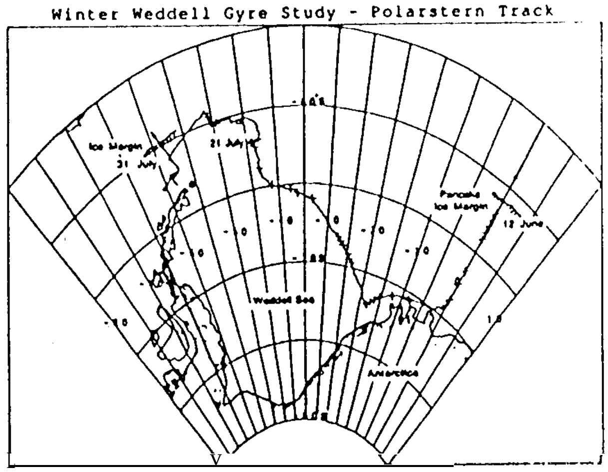

Fig, 1. WWGS 92 Polarstern track and surface sample sites (+). The icc margin was entered on [2 June '92, and finally exited on 31 July '92.

was calibrated. The height above the sea ice surface was approximately 16m, but varied as a function of the ship's draft.

Control of the radar switch logic, sampling and signal recording were performed with a Texas Instruments personal computer (PC) using tailored signal processing hardware and software developed at the University of Kansas. Red-time signal analysis of the calibration and IF signals was pcrforrncd using a Hewlett Packard (HP) Signal Analyzer in series with the PC. This enabled system performance to be monitored, as well as the occurrence of external interference from radio sources.

Table 1. FM-CW Radar Scatterometer System Specifications

Transmitter Power:	150 mW		
Center Frequency:	4.3 GHz ± 15 MHz (C-band)		
RF Bandwidth:	100 MHz		
Polarizations:	VV, HH, HV, VH		
'Antenna Beamwidths:			
Transmitting:	Parabolic: 8° (circular Gaussian)		
Receiving:	Horn	E-plane;	23° elevation
(linear pol)		H-plane;	22° azimuth
(cross pol)	KA 54:	E-plane;	50° ± 5°
		H-plane;	40° ± 4°
Calibration:	External 12" Luncbcrg-lens reflector		
Target Range:	15m - 60 m		
18m range footprint:	-1.31 x 1.44 m		

3. CALIBRATION AND SYSTEM CORRECTIONS

Here wc briefly describe procedures used to convert measured power data into absolute backscatter. These approaches arc described in further detail in [2],[3], and [4].

Internal and External Calibration

The system is internally calibrated using the PC, by recording IF power and transmitter power alternately for each radar pulse. The amplitude and the characteristics of the transmitted signal can then be taken into account in power calculations. Independent records of internal calibration readings for each measurement sample were not made using the HP signal analyzer, due to time constraints in the field. However, a frc uency gate (O-1 kHz) was applied to each sample to adjust ?or possible changes in the system throughout the experiment. The daily average of the gated power was within 1.5 dB of the mean value between June 25 and July 28 thus indicating the radar to be sufficiently stable; then the assumption of using the O-1 kHz gated power as an internal reference is reasonable.

External calibration was performed periodically using a Luneberg *lens* placed on the ice at a fixed distance from the ship. The theoretical maximum cross-section of a 12" diameter lens at 4.3 GHz is 11.38 dB [5]. The lens had a measured value σ = -7 dB (after [2]) and some performance degradation over its lifetime.

Beamshape and *Antenna Separation Correction*

Power measurements are simplified by assuming scattering is independent of azimuth angle and that received power is mainly from the elliptical illuminated area [5] centered at known range and defined by the effective half-power beamwidths given in Table 1. In estimating $\sigma^\circ(\theta)$ from the power, wc use the narrow-beam approximation [6]. Since this method has deficiencies, Wang and Gogineni [4] describe how σ° is calculated accurately by integrating the power over the antenna pattern from the full measured spectrum.

Though mounted together, the antennas do not all point to exactly rhc same spot on the surface. With a separation of 50cm and with slightly different beams, the antenna patterns overlap imperfectly and a *corrccrion* is made to account for the error in the estimation of *A*, and the 'effective' gain pattern. This correction is made using formulae for parallel Gaussian beams discussed in [7]. Together, this accounts for a correction of around 1.5 dB at nadir - falling to lcss than 1 dB at the higher incidence angles.

The point target response of a typical FM-CW radar falls off at 12 dB/octave (i.e. each time range doubles). The system hardware (i.e., STC) compensates for *6* dB/octave while the post processing of data eliminates the remaining range dependence.

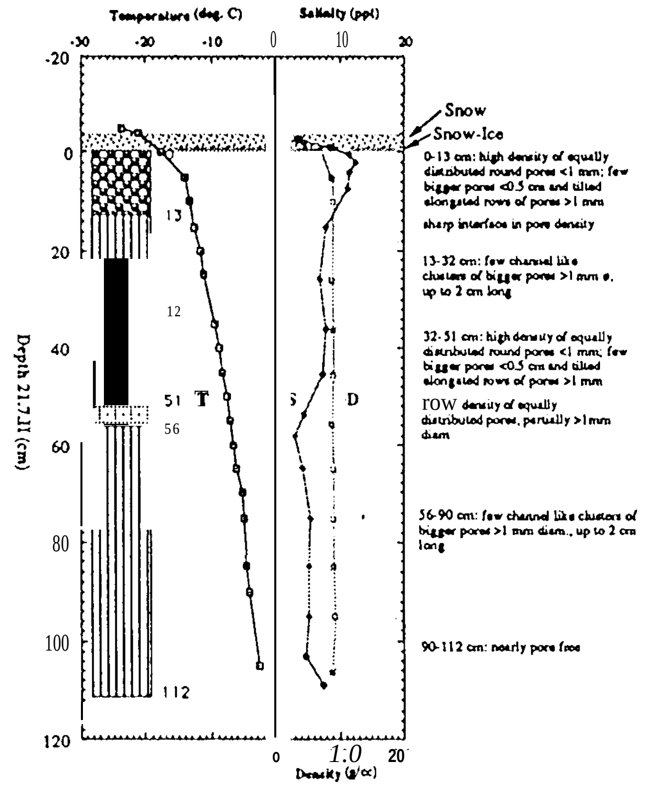

Fig. 2. physical properties of undeformed, snow-covered first-year ice on 21 July, 1992, at the site indicated in Fig. 1.

4. ICE STATION IN-SITU DATA

At each site in Fig. I detailed radar measurements were made. Estimates of σ° come from a number of independent samples, each of which is a statistical average of several thousand measurements of scattered power. Power is converted to σ° with the calibration information and corrections described in section 3. A backscatter signature is then built up from the samples of $\sigma^\circ(\theta)$. Data were recorded for a range of sea-ice types including pancake, dark nilas, white nilas, grey, first-year and second-year ice. In-situ data included physical and chemical analyses of ice core and snow samples, together with snow crystal macro-photography. Typically, such data were collected within the swath of the radar after each scan was completed. An example from a site on 21 July, is shown in Fig.2. The corresponding signature is shown in Fig. 3 as circles and crosses.

Throughout the 3 month experiment, meteorological data were acquired onboard Polarstern. Together with radiation budget calculations and oceanographic measurements, these data provide a complete picture of the top and bottom boundary conditions for the sea ice. During periods when the thermal conditions were monitored within the ice, this allowed the main components of the energy budget to be estimated. Those components critical to the physical and scattering properties of the sea ice arc the sensible and latent heat, and vapour fluxes.

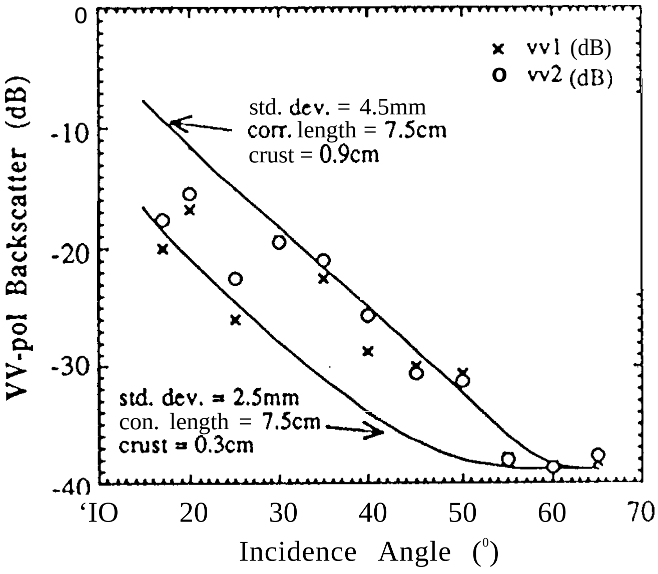

Fig. 3. C-band vv-pol scatterometer data and model simulation curves using two sets of parameters.

5. MODEL SIMULATIONS

A physical and theoretical scattering model is developed to understand the scattering shown in Fig. 3, and to provide insight into the geophysical properties regulating microwave scattering and emission and thermodynamics of sea ice. Initial tests using *in-situ snow* and ice properties suggest penetration depths into the icc shown in Fig. 2 = less than 50cm. Because of this sensitivity to the upper layers of the, snow and ice, a physical scattering model is constructed consisting of three primary layers: (i) an uppermost layer of icy snow-crust; (ii) salt-free snow with spherical crystals of varying size; and (iii) a layer of salty snow-ice resting upon an 'half-space' of first-year sea ice. The model utilizes theoretical approaches described in [8] and [9].

On 21 July, surface measurements indicated that the snow surface had a radiationally altered, wind-blown crust of density close to that of pure ice. Its temperature was close to that of the air (-24°C) and it varied from a fcw mm to 1 cm thick. In the model this layer is assigned a permittivity ε=3.17. Layer (ii) contained snow crystals of varying sizes. The temperature at 4cm depth was -20°C and the snow was assigned a dry permittivity of ε=1.68 for a mean density of 0.35g/cc. The snow particle size distribution is simulated for layer (ii) using a Rayleigh distribution with limits at a minimum grain diameter of 0.045mm and maximum diameter of 0.885 mm. Layer (iii) in contrast was salty, with a salinity of 8‰.

It is assigned a complex permittivity of $\varepsilon=2.8+j0.02$, assuming spherical brine inclusions within predominantly orbicular ice of 0.75g/cc at a temperature of -18°C. Beneath the snow-ice layer is assumed a continuous ice sheet with the characteristics noted in the upper 10cm of Fig. 2.

Measurements were made using a variety of profiling schemes to quantify the small-scale roughness of the air/snow and snow/ice surfaces. In the model it is assumed that the crust is slightly rough, but that it has an equal thickness everywhere with parallel upper and lower surfaces. This allows the second-order effects of a coherent field within the crust to be included in the computations. The roughness was large enough that Physical Optics scattering theory is valid at C-band

Simulations incorporating surface and volume scattering take into account the snow grain-size distribution and salinity of each layer together with the measured roughness and thickness of the crust. The effective extinction of each layer is computed by summing the extinction in each of 10 discretized Rayleigh grain radius bins within the overall size distribution. Layer volume scattering contributions are then added incoherently. Model simulated curves are shown in Fig. 3 in comparison with measured vv-pol σ^o data. Both curves each use the measured mean snow grain diameter of 0.3mm. The upper simulated curve indicates the scattering signature for a slightly rougher surface with crust 0.9cm thick. In contrast, the lower curve shows the situation when the crust thickness is reduced and the roughness decreased. Results indicate that the model response to the *snow* characteristics is significant. Other properties which have a large impact are the the salinity and roughness of the snow-ice interface.

The model simulations in Fig. 3 are for a situation which represents initial conditions at 19:00hrs at the beginning of a 3-day ice station. They indicate that scattering is extremely sensitive to properties which are directly influenced by the surface energy balance. A subsequent time-series of radar data indicates how the scattering signatures change as a function of the varying surface flux environment. Exchanges of heat and water vapour caused by loss or gain sensible heat and evaporative cooling appear to have a significant impact upon the physical properties of the layers with time.

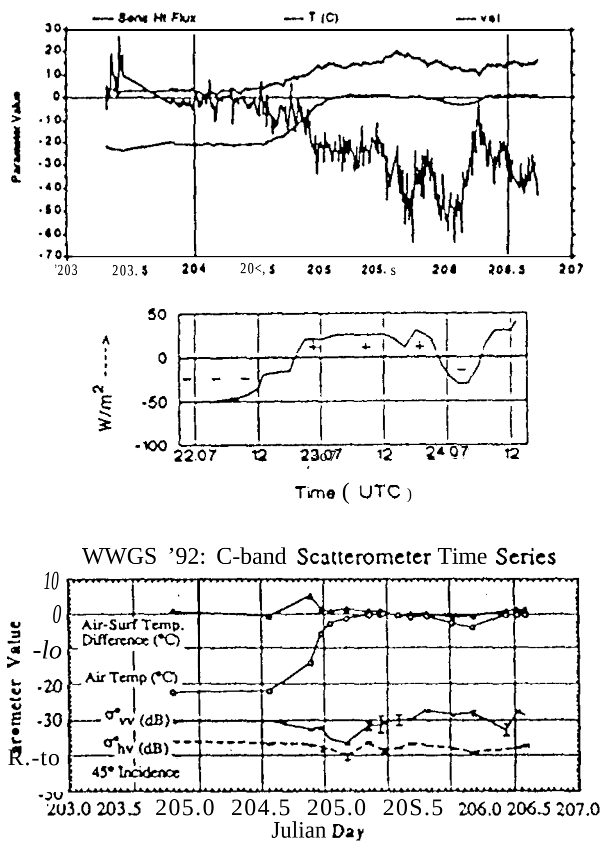

Fig. 4. C-band scatterometer time-series plotted against the sensible heat flux and total energy budget over a three-day period.

6. TIME-SERIES DATA

Another result from WWGS'92 field experiment in Fig. 4 shows simultaneous energy budget and scatterometer time-series data lasting from 21 to 24 July, 1992. The signature shown in Fig. 3 represents the starting point in this time-series of data at Julian Day 2/3.79. The upper panel of *Fig.* 4 shows the sensible heat flux as it varied with surface air temperature and wind velocity from day 203 (21 July,'92) to day 206 (24 July,'92). The middle panel shows the overall energy budget of the ice (by courtesy of W. Frieden of Hannover University, Germany) with "-" illustrating net outgoing heat fluxes of heat (and vice-versa for "+"). The lowermost panel shows the C-band, scatterometer data in response to the heat fluxes together with air and ice surface temperature traces.

The period of observations is marked by a 23°C change in air temperatures caused by the passing of a low pressure front. The situation led to a swing from net negative heat flux and upward vapour flux, to net positive heat flux and initiation of surface melting. Several dB variability in vv-polarized backscatter indicate several orders of magnitude change in scattering over the range of temperatures and resulting heat flux regimes indicated. The change in heat flux regime causes a reduction in vv and hv backscatter which lags the onset of net heat gain to the snow by a few hours. High winds and a brief period of cloud-free night at Julian Day 206.2 encourage evaporative cooling and a local maximum in the values of w and hv-pol backscatter.

The example in Fig. 4, indicates that regional sea-ice surface properties reflect the balance between atmospheric or oceanographic forcing; and time-series data reflect transformations in the surface heat and vapour flux environment. It proposed that with the aid of weather analysis fields for specifying boundary conditions, the satellite and surface data will be used in models to generate regional scale heat flux estimates.

& ACKNOWLEDGEMENTS

Special thanks go to Thomas Viehoff, Peter Lemke and Christian Wamser of the AWI, and to Prasad Gogineni for the radar. Work was performed at the Jet Propulsion Laboratory, California Institute of Technology, under contract to the National Aeronautics and Space Administration. Robert Thomas (SED) and John Theon (SEP) of NASA Headquarters supported the Antarctic field program.

9. REFERENCES

[1] Haas, C., T. Viehoff, and H. Eicken, Sea-ice conditions during the Winter Weddell Gyre Study 1992 ANT X14 with R/V Polarstern: Shipboard observations and AVHRR satellite imagery, *W. I Berichte aus dem Fachbereich Physik*, 34, 1992.

[2] Bredow, J. W., A laboratory investigation into microwave backscattering from sea ice, Unpublished Ph.D. Thesis, University of Kansas, 173pp., 1989.

[3] Onstott, R.G., R.K. Moore, S.P. Gogineni, Y.S. Kim, and D. Il. Bushnell, Helicopter-borne scatterometer, *RSL Tech. Report*, 331-24, Univ. Kansas Center for Research, Inc., Lawrence, KA, 1982.

[4] Wang, Q., and S.P. Gogineni, A numerical procedure for recovering true scattering coefficients from measurements with wide-beam antennas, *RSL Tech. Report, 8240-2*, Univ. Kansas Center for Research Inc., Lawrence, KA, *26pp.*, 1991.

[5] Ulaby, F.T., R.K. Moore, and A.K. Fung, Microwave *Remote* Sensing: *Active and Passive, vol.* II, Artech House, Norwood, MA., 1064pp., 1982.

[6] Gogineni, S., R.K. Moore, Q. Wang, A. Gow, and R.G. Onstott, Radar back-scatter measurements over saline ice. *Int. J. Remote* Sensing, 11,4, 603-615, 1990.

[7] Moore, R. K., Effect of pointing errors and range on performance of dual pencil-beam scatterometers. *IEEE Trans. Geosci. and Remote Sensing*, 23.901-905.1985.

[8] Dierking, W., Sensitivity studies of selected theoretical scattering models with applications to radar remote sensing of sea ice, *A WI Berichte aus dem Fachbereich Physik, 33*, 113pp., 1992.

[9] Winebrenner, D. P., J. Bredow, M.R. Drinkwater, A.K. Fung, S.P. Gogineni, A.]. Gow, T.C. Grenfell, H.C. Han, J.K. Lee, J.A. Kong, S. Mudaliar, S. Nghiem, R.G. Onstott, D. Perovich, L. and R.D. West, Microwave Sea Ice Signature Modeling, In Microwave *Remote Sensing of Sea-Ice, (Ed.)* F.D. Carsey, American Geophysical Union, Geophysical Monograph 28, Chapter 8, 137-175, 1992.